Interplay between structural, magnetic, and electronic properties in a FeO/Pt(111) ultrathin film

Livia Giordano* and Gianfranco Pacchioni
Dipartimento di Scienza dei Materiali, Università di Milano-Bicocca, via Cozzi, 53-20125 Milano, Italy

Jacek Goniakowski
Institut de Nanosciences de Paris, Universitées 6-7 and UMR CNRS 7588, 140 Rue de Lourmel, 75015 Paris, France

Niklas Nilius, Emile D. L. Rienks, and Hans-Joachim Freund
Department of Chemical Physics, Fritz-Haber Institut der Max-Planck Gesellschaft, Faradayweg 4-6, D-14195 Berlin, Germany
(Received 7 May 2007; revised manuscript received 4 July 2007; published 14 August 2007)

We have investigated the magnetic and electronic properties of a FeO film grown on Pt(111). Coupling first-principles density-functional theory calculations with scanning tunneling microscopy (STM) measurements we have identified the principal mechanisms for the structural and electronic characteristics observed in the Moiré unit cell formed between oxide film and metal support. We show that both free and supported FeO(111) monolayers present an antiparallel alignment of the magnetic moments. Due to the lattice mismatch between Pt(111) and the FeO film, the interface properties are different in different regions of the supercell. The resulting modulation of the structural and electronic properties of the film is determined by the strength of the film-substrate interaction in various regions of the supercell. In particular, for the Fe-top site, where this interaction is weak, there is a small rumpling of the FeO layer which increases the interface separation. In correspondence of this structural modification, we observe a change in the work function, coherent with the most recent experimental findings. Our results show that a good agreement with the experimental interpretation of the work function modulation and of the STM images can be obtained only within the more robust, nonpseudomorphic computational models.

DOI: 10.1103/PhysRevB.76.075416 PACS number(s): 73.30.+y, 75.70.Ak, 68.55.−a, 68.37.Ef

I. INTRODUCTION

Oxide ultrathin films on metals represent a class of materials with promising properties for applications in microelectronics, magnetic devices, and as support in catalysis.[1–4] Films of a few atomic layers may exhibit structures that are completely different from those of bulk oxides and display many different phases, depending on the growth conditions.[5–8] In some cases, even though the structural and electronic properties of the ultrathin films are similar to those of the massive material, the films may indeed display unexpected properties. For instance, it has been shown that MgO thin films on Mo(100) or Ag(100) substrates may exhibit modified reactivity towards adsorbed molecules or metals.[9–12]

An iron oxide film grown on Pt(111) presents some additional points of interest. Indeed, the FeO(111) layer, experimentally grown for the first time by Vurens *et al.*,[13] has a polar orientation. The field of polar oxide surfaces has received growing attention in recent years.[14–19] In fact, it has been shown that the surface polarity can be healed by nonstoichiometric reconstructions, metalization of the surface layer, or by absorption of charged species. Furthermore, metal-oxide interfaces may have a role in stabilizing polar surfaces.[20,21] The situation is qualitatively different for ultrathin films: rather flat, unreconstructed MgO(111) ultrathin films have been successfully stabilized on Ag(111).[22,23] For these nanostructures the polarity may be compensated by a structural transformation.[24] The iron oxide on Pt(111), on the other hand, presents a nonvanishing Fe-O rumpling and therefore can be considered as a nanosystem in which uncompensated polarity remains.[25] The structure of the iron oxide film has been extensively characterized by scanning tunneling microscopy (STM) and x-ray photoelectron diffraction,[26–31] while the STM images have been interpreted with the help of theoretical results.[32] The film has a bilayer structure, where the iron atoms are at the interface, while the oxygen atoms form the surface layer. The experimental interlayer distance between the Fe and O layers, 0.68 Å,[27] is reduced by almost 50% with respect to the corresponding bulk FeO interplane distance. On the other hand, the in-plane lattice parameter of 3.1 Å is slightly larger than the corresponding bulk value of 3.0 Å. Relatively large (11%) mismatch between the oxide layer and the Pt substrate (in-plane lattice parameter 2.77 Å) results in a Moiré pattern with a periodicity of about 26 Å.[13,27,29]

The corrugation of the Moiré pattern, quantified recently by STM images, has been related to the variation of the surface potential within the Moiré unit cell.[31] The interaction of the FeO(111) film with metal layers and particles has also been addressed.[33–35] It has been pointed out that, atoms adsorbed on regions of the oxide film that present a different register with the substrate may exhibit a different adsorption strength. In fact, the Moiré pattern provides a template for self-organization of gold atoms.[35]

An additional reason of interest for this system is the magnetic nature of the oxide. At ambient pressure and low temperature, FeO assumes a distorted $B1$ structure.[36] The rhombohedral distortion is due to the type-II antiferromagnetic (AFM) order (individual atomic moments are aligned in {111} ferromagnetic layers, with adjacent layers having antiparallel spins). If the same magnetic ordering were maintained in the thin film, one would expect a ferromagnetic (FM) FeO(111) overlayer. On the other hand, it has been

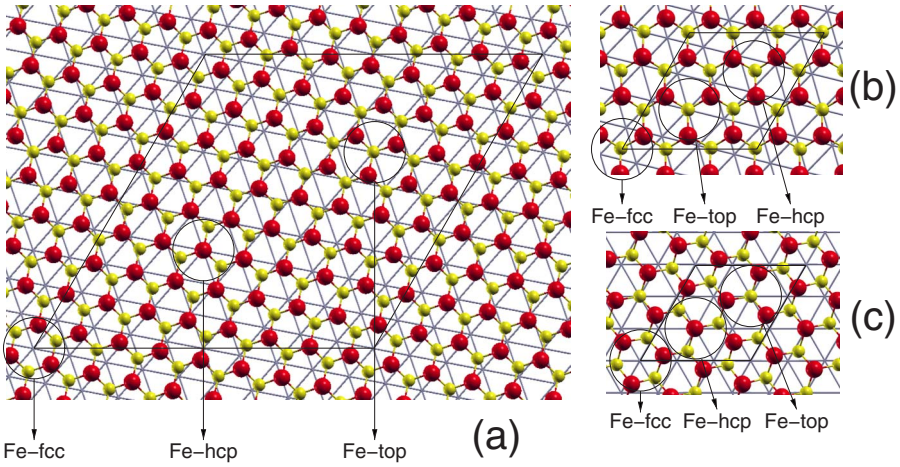

FIG. 1. (Color online) Top view of (a) the experimental Moiré unit cell, (b) NP1 [superposition of (3×3)-FeO(111) and $(\sqrt{13}\times\sqrt{13})R14°$-Pt(111)], and (c) NP2 [superposition of $(\sqrt{7}\times\sqrt{7})R19°$-FeO(111) and (3×3)-Pt(111)] unit cells used in the calculations for the FeO/Pt(111) film. Large (red) spheres, O atoms; small (yellow) spheres, Fe atoms. The intersections between the (gray) lines represent the position of the surface Pt(111) atoms.

shown that (homoatomic) magnetic monolayers on transition metal substrates may have magnetic structures which are completely different from the bulk materials.[37,38] This is particularly true for triangular lattices where the AFM interaction is frustrated by the symmetry of the system and can result in complex magnetic structures.[39]

In this paper we investigate the relative stability of various FeO/Pt(111) interface structures, taking into account different magnetic configurations. To this end we perform a full geometrical optimization and we use both pseudomorphic and nonpseudomorphic models of the interface. We show that changes in work function of the system occur because of the different positions of the atoms in the oxide layer with respect to the Pt substrate. We also analyze the mechanisms responsible for the modulation of the surface potential within the Moiré unit cell. Finally, we discuss the effects responsible for the contrast found in STM images of FeO/Pt(111).

II. EXPERIMENTAL AND COMPUTATIONAL TECHNIQUES

A. Computational methods and models

Density-functional theory (DFT) methods fail in describing the electronic structure of transition metal oxides, when these are dominated by the on-site Coulomb repulsion between d electrons. For instance, the DFT prediction of a metallic ground state for bulk FeO contradicts the experimental finding of insulating behavior. In order to overcome this shortcoming, previous studies on bulk FeO have been carried out within the LDA+U method or with hybrid functionals.[40–44] The DFT+U approach combines DFT with a Hubbard Hamiltonian for the Coulomb repulsion and exchange interaction. Also the FeO(111) surface has been recently studied with the LDA+U approach.[45] In the present study we use the DFT+U approach, as formulated by Dudarev[46] and implemented in the VASP code,[47,48] using the generalized gradient approximation (GGA) and the Perdew-Wang 91 (PW91) functional[49] [plane wave basis set with the kinetic energy cutoff of 400 eV, and projected augmented wave (PAW) method[50,51]]. Similarly to the existing studies on iron oxides (hematite in the GGA+U approach[52]), we obtain a satisfactory description of distorted $B1$ bulk properties for $U=4$ eV and $J=1$ eV. In particular, we find a type-II AFM insulating ground state with a band gap of 1.4 eV in line with previous calculations.[40–42,44]

Atomic charges reported in the paper are obtained within the scheme of charge density decomposition proposed by Bader.[53] Magnetic moments of ions are estimated from electronic densities projected into atomic spheres. The work function ϕ measures the difference between the vacuum level and the Fermi energy. The FeO-induced modification, $\Delta\phi$, refers to a fully relaxed clean Pt(111) surface at the same lattice parameter.

A direct simulation of the experimentally observed FeO/Pt(111) interface structure is beyond the present computational possibilities because of the too large unit cell, Fig. 1(a). In the Moiré unit cell three regions can be identified along its diagonal, which have been classified in the literature with respect to the position of the Fe atoms and the Pt(111) substrate. Between these regions of the experimental unit cell both Fe and O ions occupy intermediate positions with respect to the Pt substrate. In the "Fe-fcc" region both Fe and O atoms are in threefold hollow position with respect to the Pt substrate, and the Pt surface atoms are visible below the FeO layer in the center of the hexagons formed by the FeO overlayer. On the other hand, in the "Fe-hcp" region the O atom is just on-top of a surface Pt atom, while the Fe atom adsorbs in the hcp position. Finally, in the "Fe-top" region the O atom is in the fcc position and the Fe atom is on-top of a surface Pt, Fig. 1(a).

To investigate the properties of this system we have used two different strategies. We first performed a series of separate model calculations on pseudomorpic lattices, representing different bonding modes of the oxide layer on the Pt(111) substrate. In these models that have already been used in the past the FeO(111) and Pt(111) lattices are aligned and the substrate has been expanded to match the experimental lattice parameter of FeO(111) (3.1 Å).[32–34] In each pseudomorphic model a different register between the oxide film and the metal substrate has been considered: Fe-top, Fe-fcc, and Fe-hcp. With respect to previous theoretical studies of pseudomorphic models we have considered here the effect of the magnetic ordering on the properties of the FeO film. In particular, in addition to the (1×1) ferromagnetic solution,

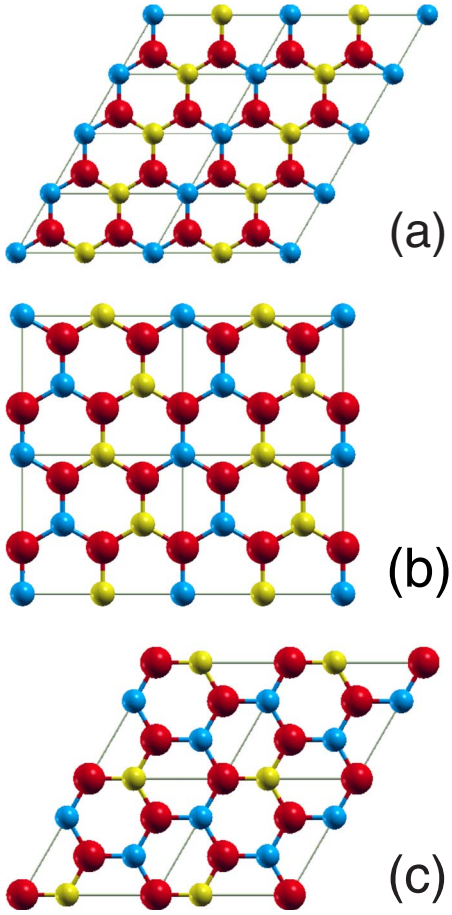

FIG. 2. (Color online) Magnetic structures of the FeO(111) monolayer: (a) row-wise RW-AFM-(2×1), (b) zig-zag ZZ-AFM-(2×2), (c) CO-AFI-$(\sqrt{3}\times\sqrt{3})R30°$ collinear correspondent of the 120°-Néel structure. Large (red) spheres, O atoms; small (yellow and blue) spheres, Fe atoms with opposite magnetization.

we have also considered two AFM orderings, Fig. 2, a row-wise RW-AFM-(2×1) structure, and a zig-zag ZZ-AFM -(2×2) structure. Moreover, we have considered the $(\sqrt{3}\times\sqrt{3})R30$ collinear equivalent of the 120°-Néel structure typical of triangular lattices. This has an antiferrimagnetic ordering with 2/3 of the cations with the same magnetization and 1/3 with opposite magnetization, Fig 2(c). This magnetic structure will be named CO-AFI. Notice that the RW-AFM and CO-AFI structures are the collinear equivalents of magnetic structures which have been found to be energetically favorable for hexagonal Mn and Cr monolayers on Cu(111).[54]

Two more realistic nonpseudomorphic (NP) interface models have been considered [Figs. 1(b) and 1(c)]. While these do not correspond to the supercell observed experimentally, and as such are still an approximation of the real interface, they are much closer to the reality. The first one consists of a superposition of (3×3)-FeO(111) and $(\sqrt{13}\times\sqrt{13})R14°$-Pt(111) structures, hereafter referred to as NP1 surface cell, Fig. 1(b). Similarly to the real one, this structure contains the three high-symmetry adsorption sites for the Fe atom (top, fcc, and hcp) and some other sites, such as the bridge ones. As a consequence, most oxygen atoms are somewhat off the high symmetry sites. Furthermore, this cell can accommodate the CO-AFI magnetic structure of the FeO(111) film which is the most stable one among those considered for the pseudomorphic layers (see below). The use of the experimental FeO(111) lateral lattice parameter produces a residual (7%) strain between the FeO and Pt(111) lattices which, as in the case of pseudomorphic models, is accommodated by a lateral contraction of the Pt substrate. Since the contracted Pt substrate reconstructs easily upon FeO adsorption, we have constrained its relaxation, fixing the Pt atoms at their (relaxed) clean surface positions. This constraint on the Pt surface makes this model not fully satisfying. For this reason we have considered a second nonpseudomorphic structure (NP2) consisting of a superposition of $(\sqrt{7}\times\sqrt{7})R19°$-FeO(111) and (3×3)-Pt(111) structures. The main advantage of this structure is the small (1%) lattice mismatch (once again accommodated on the metal substrate), which allows us to fully relax the structure, including the Pt substrate. As we will show below the removal of the interface constraint is crucial to correctly reproduce the transition in the contrast observed in the experimental STM images. Also in this unit cell we can identify the three high symmetry regions of the experimental Moiré unit cell, although in this case the Fe ions are slightly off symmetry in the fcc and hcp regions, Fig. 1(c). The main disadvantage of this structure is that it cannot accommodate AFM or simple AFI structures, as it contains seven Fe atoms and therefore a magnetic defect.

In all the calculations we have used a supercell slab approach, with the Pt(111) substrate represented by five atomic layers and the oxide layer adsorbed on one side of the metal slab only. The slabs were separated by at least 10 Å of vacuum and a dipole correction has been applied in order to eliminate the residual dipoles in the direction perpendicular to the surface. While all atomic coordinates of the FeO film were optimized in the two nonpseudomorphic cells, in the pseudomorphic models only the vertical atomic positions have been relaxed. The corresponding atomic forces were considered to be converged when smaller than 0.01 eV/Å. The Brillouin zone of the (1×1) unit cell (3.1 Å$\times$3.1 Å) was sampled on a $(6\times6\times1)$ Monkhorst-Pack grid, and an equivalent k-point sampling was used for larger unit cells.

B. Experiment

Thin FeO films are prepared by depositing one monolayer of Fe onto a Pt(111) surface, which is cleaned before by repeated sputter and anneal cycles. The iron is then oxidized in 10^{-6} mbar O_2 at 1000 K, resulting in the formation of a well-ordered FeO film as verified by low-energy electron diffraction (LEED). The STM images are obtained with a home-built instrument operated at liquid-helium temperature. All images are taken in the constant current mode with the bias referring to the sample.

III. RESULTS AND DISCUSSION

A. Unsupported FeO(111) monolayer

The structural properties of the unsupported FeO(111) layer depend only slightly on the magnetic configuration. For

TABLE I. Structural and electronic properties of an unsupported FeO(111) monolayer as a function of the magnetic configuration.[a]

Structure	ΔE	μ_{Fe}	μ_O
FM-(1×1)	0	3.7	0.2
RW-AFM-(2×1)	−0.16	±3.6	±0.1
ZZ-AFM-(2×2)	−0.16	±3.6	±0.1
CO-AFI-$(\sqrt{3}\times\sqrt{3})R30°$	−0.16	−3.5, 3.6, 3.6	±0.1
NCO-120°-Néel-$(\sqrt{3}\times\sqrt{3})R30°$	−0.18	±3.6	0.0

[a]ΔE (eV/FeO unit) is the energy difference with respect to the FM-(1×1) configuration (a negative value indicates a more stable structure); μ is the magnetic moment in Bohr magnetons (μ_B).

all magnetic structures considered the FeO film assumes a perfectly planar geometry, with the in-plane lattice parameter about 8% larger than that of a bulk-truncated FeO layer. This corresponds to Fe-O and Fe-Fe distances of 1.90 Å and 3.29 Å, respectively (2.15 Å and 3.04 Å in bulk FeO). While the FM structure is clearly unfavorable (by about 0.15 eV/FeO unit), the two AFM and the CO-AFI-$(\sqrt{3}\times\sqrt{3})R30°$ structures are isoenergetic, see Table I. Inclusion of noncollinearity leads to the NCO-120°-Néel -$(\sqrt{3}\times\sqrt{3})R30°$ magnetic structure and brings an additional stabilization of about 0.02 eV/FeO unit with respect to the collinear CO-AFI-$(\sqrt{3}\times\sqrt{3})R30°$ solution, Table I. The calculated Fe magnetic moments ($\mu_{Fe}=3.6\mu_B$ in bulk FeO) depend little on the particular magnetic structure.

B. FeO/Pt(111) monolayer: pseudomorphic models

We start our discussion from the pseudomorphic models, considering three magnetic structures, FM-(1×1), RW-AFM-(2×1), and CO-AFI-$(\sqrt{3}\times\sqrt{3})R30°$. For each one of these interfaces, we have considered different positions of the Fe atoms with respect to the Pt(111) substrate. Six possible interface structures have been initially considered, with the Fe and O atoms in fcc, hcp, and top positions. Among them, only three turned out to be fully inequivalent and, in the following, we classify them conventionally by the respective position of the Fe atom (in parentheses is that of the O atom): Fe-fcc (O-hcp), Fe-hcp (O-top), Fe-top (O-fcc), see Table II.

The preference for the antiparallel orientation of the magnetic moments is maintained also for the supported films, Table II. The associated energy gain is clearly site-dependent, weaker for the Fe-hcp or Fe-fcc hollow sites and stronger for the Fe-top site (where it is close to that in the free FeO layer). Although the energy differences are small, we find a moderate preference for the CO-AFI-$(\sqrt{3}\times\sqrt{3})R30°$ magnetic structure.

An advantage of the pseudomorphic models is the possibility to estimate the relative stability of the different interface structures, Table II. The Fe-fcc sites, with both Fe and O ions in the Pt(111) hollow sites, are always preferred. In the case of the somewhat less stable Fe-hcp configuration, the O atom is exactly above the surface Pt atom (on-top adsorption site). The Fe-top configuration is the least stable one, with O

TABLE II. Structural and electronic properties of FeO/Pt(111) pseudomorphic models (experimental lattice parameter of 3.10 Å).[a]

	ΔE	$d_{Fe\text{-}O}$	z_{FeO}	Δz	μ_{Pt}	$\Delta\phi$
			FM-(1×1)			
Fe-fcc	0	1.93	2.43	0.73	0.3	+0.96
Fe-hcp	0.25	1.93	2.49	0.74	0.3	+0.78
Fe-top	0.36	1.89	2.78	0.62	0.3	+0.09
			RW-AFM-(2×1)[b]			
Fe-fcc	−0.09	1.92 (1.93)	2.44 (2.42)	0.70 (0.68)	0.1 (0.1)	+0.54 (+0.46)
Fe-hcp	0.11	1.93 (1.93)	2.49 (2.47)	0.72 (0.65)	0.1 (0.1)	+0.35 (+0.13)
Fe-top	0.14	1.88 (1.91)	2.77 (2.74)	0.60 (0.51)	0.3 (0.3)	−0.31 (−0.60)
			CO-AFI-$(\sqrt{3}\times\sqrt{3})R30°$			
Fe-fcc	−0.12	1.92	2.44	0.69	0.2,0.2,0.2	+0.40
Fe-hcp	0.06	1.93	2.50	0.71	0.2,0.2,0.2	+0.31
Fe-top	0.14	1.89	2.78	0.60	−0.2,0.3,0.3	−0.37

[a]ΔE (eV/FeO unit) represents the energy difference with respect to the Fe-fcc adsorption of the FM(1×1) phase; d(Fe-O) (Å) is the Fe-O bond length; z_{FeO} (Å) is the average adsorption height; Δz (Å) is the layer rumpling; μ_{Pt} (μ_B) is the magnetic moment on surface Pt; $\Delta\phi$ (eV) is the work function change with respect to Pt(111).

[b]Values in parentheses are obtained for the optimized lateral lattice parameter (Fe-fcc, $a=3.12$ Å; Fe-hcp, $a=3.14$ Å; Fe-top, $a=3.18$ Å).

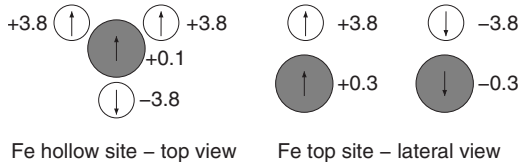

FIG. 3. Schematic representation of the FeO induced magnetization on the Pt surface top layer. The values represent the magnetic moments (μ_B). Large gray spheres, Pt atoms; small white spheres, Fe atoms.

atoms in surface fcc sites. The absolute adsorption energies for the CO-AFI-($\sqrt{3}\times\sqrt{3}$)$R30°$ configuration, computed with respect to the fully optimized unsupported FeO(111) layer, go from 0.86 eV/FeO unit (Fe-fcc) to 0.60 eV/FeO unit (Fe-top).

In all models and configurations considered, the supported FeO layer has a considerable surface rumpling ($\Delta z = z_O - z_{Fe}$) with oxygen ions relaxing outwards (positive rumpling), Table II. The rumpling depends little on the magnetic order of the FeO layer and on the particular interface geometry. The clear exception is the Fe-top interface structure, where the rumpling is much smaller (about 15%). The increase of the lateral lattice parameter for the Fe-top structure (a=3.18 Å for the laterally optimized configuration) results in a further reduction of the rumpling, Table II. Also the average interface distance, $z_{FeO}=(z_{Fe}+z_O)/2$, depends only slightly on the magnetic order in the FeO layer, but is quite sensitive to the interface geometry, Table II. The interface distance follows the behavior expected from a hard-spheres model[31] as already known for reverse metal on oxide systems:[55] z(Fe-top) $\gg z$(Fe-hcp) $> z$(Fe-fcc) and correlates with the relative stability of the corresponding configurations. The Fe-O distances within the layer show a weak expansion with respect to the unsupported case, an effect which is negligible for the Fe-top configuration where the interaction with the substrate is weaker.

The electronic structure of the interface is characterized by an electron transfer of 0.2–0.3e from the FeO film towards the Pt(111) surface. This charge transfer is practically independent of the magnetic configuration and its strength correlates with the interface distance z_{FeO}. Also, the local magnetic moments on the Fe and O ions [μ(Fe)=3.8μ_B, μ(O)=0.1μ_B] are basically independent of the magnetic ordering and the interface structure. However, an interesting effect is observed on the Pt atoms of the metal substrate. The deposition of the magnetic FeO layer induces a magnetization of the Pt(111) substrate, although limited to the Pt top layer. The largest induced magnetization on Pt, μ(Pt) =0.3μ_B, is found for the Fe-top configuration. This is due to the strongly interacting Fe neighbor, Fig. 3. In the other configurations, the contribution of several neighboring Fe ions may produce a constructive or destructive effect on the spin of the surface Pt atoms, Fig. 3. As a consequence, the resulting magnetization on these sites depends strongly on the magnetic structure of the FeO overlayer, Table II, and on the relative position of the oxide film. The weak site-dependent magnetization on Pt could have a role in the zero-bias conductance anomaly observed by scanning tunneling spectroscopy in the Fe-top region of the Moiré pattern, which is tentatively assigned to the Kondo effect.[56]

Turning now to the estimation of the change in work function $\Delta\phi$ induced by the oxide layer, we note that $\Delta\phi$ depends strongly on the structure of the interface and on its magnetic order, and that its modulation is mainly due to the peculiarity of the Fe-top structure. For instance, for the most stable CO-AFI-($\sqrt{3}\times\sqrt{3}$)$R30°$ structure, $\Delta\phi$ is 0.30–0.40 eV for most configurations, except for the Fe-top site, where $\Delta\phi$ is −0.37 eV, Table II. In the next section we will present results of a more realistic model of the FeO/Pt system and show that this particular behavior can be assigned to the peculiar structure of the Fe-top configuration.

In summary, regardless of the magnetic order, the energetic stability shows a clear trend in favor of the hollow adsorption sites, especially if compared to the Fe-top one. The AFM and AFI orderings are very similar in energy and clearly more stable than the FM one. Our results on the pseudomorphic models, although consistent with the results of ferromagnetic resonance spectroscopy measurements, which show that the film is not ferromagnetically ordered,[56] do not exclude a possible existence of a more complex magnetic ordering, driven by the local structure of the interface. The calculated overall structural characteristics agree very well with the experimental estimates.[27] In all models considered, the Fe-top configuration presents a clear structural peculiarity: the interaction between the FeO and the Pt substrate is the weakest, so that the FeO film adsorbs with the longest distance from the Pt surface and has the smallest rumpling. The Fe-top geometry produces a strong reduction of the work function, while ϕ increases for the other interface structures.

C. FeO/Pt(111) monolayer: nonpseudomorphic models

We turn now to the results obtained for the two nonpseudomorphic models (NP1 and NP2): we briefly comment on their magnetic and electronic characteristics and analyze the differences of their atomic structure with respect to the models described above. Then, we focus on the experimental field-emission STM results, which we analyze in terms of local variation of the work function. Finally, we use simulations within the Tersoff-Hamann approach[57] to identify the origin of bias-dependent contrast changes in the low-bias STM images of the FeO Moiré cell.

1. Magnetic and geometric structure

The preference for an antiparallel orientation of the Fe magnetic moments found for the pseudomorphic models is maintained also for the NP1 structure. In this case, the three possible antiferrimagnetic structures considered (characterized by a different register of the magnetic moment of the Fe ions with respect to the Pt substrate) are nearly isoenergetic and about 0.2 eV/FeO more stable than the corresponding FM solution. In analogy with the unsupported case, we expect that the stability will be further enhanced by noncollinear effects (120°-Néel structure). Three alternative antiferromagnetic structures were considered also for the NP2 cell. Since this interface model, composed of seven Fe ions, con-

TABLE III. Structural and electronic properties of the FeO/Pt(111) monolayer in the NP1 and NP2 unit cells.[a]

	l	$d_{\text{Fe-O}}$	z_{FeO}	Δ_z	δV (eV)
			AFI-NP1		
Fe-fcc	3.09	1.95	2.66	0.77	0.07
Fe-hcp	3.09	1.94	2.66	0.80	0.14
Fe-top	3.12	1.90	2.82	0.52	−0.15
Average cell	3.10	1.91	2.73	0.67	0.00
			AFI-NP2		
Fe-fcc	3.00	1.92	2.51	0.71	0.00
Fe-hcp	3.09	1.93	2.61	0.75	0.13
Fe-top	3.12	1.89	2.77	0.47	−0.17
Average cell	3.10	1.92	2.67	0.67	0.00

[a]l is the Fe-O lattice parameter (Å); $d_{\text{Fe-O}}$ is the Fe-O bond length (Å); z_{FeO} is the interface distance (Å); Δz is the rumpling (Å); δV (eV) is the modulation of the electrostatic potential estimated as a difference between the local (V) and the cell average ($\langle V \rangle$) values at a distance of 5 Å from the Pt(111) surface.

tains necessarily a magnetic defect (a local ferromagnetic alignment), we have positioned the latter at different high-symmetry sites: Fe-top, Fe-fcc, and Fe-hcp.

In both models the calculated energetic and structural characteristics of different antiferromagnetic solutions are very similar. Conversely, the local magnetic order may have a non-negligible effect on the fine structure of the calculated STM images at the lowest bias. We remind that the coupling between the local interface structure and the magnetism, already discussed for the pseudomorphic layers, Table II, suggests the possible existence of more complex magnetic structures, with the local magnetic order driven by the specific position of the Fe and Pt lattices in the Moiré cell. For simplicity, in the following we describe only the energetically most favorable solution for each of the two NP models.

The structural properties of the FeO layer computed with the nonpseudomorphic models, Table III, are reminiscent of those of the pseudomorphic layers. Calculated average rumpling corresponds to about $\frac{1}{2}$ of the bulk FeO interlayer spacing and correlates well with the experimental estimate.[27] Again, the Fe-top interface region presents a structural peculiarity: the interaction between FeO and the Pt substrate is weak, resulting in a long interface distance, a particularly small rumpling, and Fe-O bond lengths close to those of the unsupported FeO(111) film. While the modulation of rumpling is more pronounced in the case of the nonpseudomorphic interface structures, Table III, the modulations of the local lattice parameter, the adsorption height, and the Fe-O bond lengths are much smaller than for the pseudomorphic cells. This may be ascribed to the lateral bonding which prevents perfect "wetting" of the surface by the FeO layer. We notice that while the average rumpling is only little modified, the calculated average adsorption height is considerably larger in the NP models. The difference between average adsorption heights obtained for the NP1 and NP2 interfaces is due to the artificial lateral constraint imposed on the substrate in the NP1 model, which results in a weaker FeO-Pt interaction, Table III.

2. *Work function*

A rough estimate of the local work function can be obtained experimentally when operating the STM in the field-emission regime (bias voltage above 4 V). In this mode, electrons leave the tunnel barrier and propagate as free carriers between tip and sample. The differential conductance in the tip-sample gap is now determined by field-emission resonances, which can be viewed as standing electron waves formed in the classically accessible part of the gap. Their energy position sensitively depends on the local work function of the sample material. The increase in conductance due to electron transport through field-emission resonances is converted into a retraction of the tip from the surface (corresponding to an increase in apparent height) in order to maintain a constant tunnel current. In STM images taken at 4.5 V, Fig. 4(a), the domains marked by a circle are imaged with largest apparent height, indicating that the first field-emission resonance is reached in this region at relatively small bias due to its lower work function. The second brightest area is the one marked by a square. Here, the first field-emission

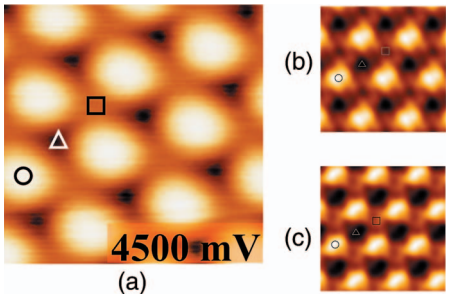

FIG. 4. (Color online) (a) STM topographic images of FeO on Pt(111) taken at 4500 mV (I_t=0.1 nA, 8.6×8.6 nm^2). (b) and (c) Map of the electrostatic potential ($-\delta V$) (averaged in circle of a radius of 2 Å, 2.5×2.5 nm^2) calculated in the (b) NP1 and (c) NP2 unit cells of the FeO/Pt(111) film. The symbols represent the position of the high-symmetry Fe ions: Fe-top (circle), Fe-hcp (triangle), and Fe-fcc (square).

resonance occurs at slightly higher bias. The triangular domains appear darkest, because field-emission resonances in this area open at considerably higher energy and the differential conductance is still small. From spectroscopic measurements, the energy position of the first field-emission resonance is determined to 4.5 V, 4.8 V, and 5.1 V for the regions marked by a circle, a square, and a triangle, respectively. This sequence also provides a measure for the local work function, which increases in the same order for the different domains.

Figure 4 presents also the calculated modulation of the electrostatic potential $\delta V = V - \langle V \rangle$ in the different regions of the two NP Moiré cells. Figures 4(b) and 4(c) show $-\delta V$ evaluated for a distance of 5 Å from the Pt surface (see also Table III) and allow an assignment of the experimental regions (circle, triangle, square) to the real Fe-Pt stacking. Both interface models account satisfactorily for the quantitative and qualitative features of the experimental image. In line with the experimental interpretation,[31] the calculated work function reduction is largest for the Fe-top sites and smallest for the Fe-hcp ones. The estimated modulation of δV $[V(\text{top}) - V(\text{hcp}) = 0.3$ eV] is slightly underestimated compared to the experiment $[V(\text{top}) - V(\text{hcp}) = 0.6$ eV]. Although considerably attenuated, δV behaves similarly to $\Delta\phi$ calculated in the pseudomorphic models, Table II. However, an overall decrease of the electrostatic potential at the Fe-fcc site in the NP models results in an inversion of δV between Fe-hcp and Fe-fcc sites with respect to the corresponding $\Delta\phi$ obtained with the pseudomorphic models. Apparently, only the NP models are consistent with the interpretation of the STM images taken in the field-emission regime.

Several effects contribute to the work function of the FeO/Pt system. Due to the outward relaxation of oxygen atoms, the dipole moment of the FeO film increases the work function. On the other hand, the dipole moment of the interface reduces it due to the electron transfer from the FeO layer to the Pt substrate. Similar conlcusions have been reported based on first-principles calculations to explain the corrugation in the work function for NaCl films on Ag(100).[58] Also the compression of the metal electron density tail by the oxide film acts towards a decrease of the work function.[59,60] In this context, the singular negative value of δV for the Fe-top configuration can be attributed to the cooperative effect of the smallest rumpling (the smallest dipole of the FeO film) and the largest interface separation (the largest interface dipole). On the contrary, the Fe-hcp (Fe-fcc) geometry has the largest rumpling (smallest interface separation). Our results show that δV cannot be assigned to the effect of rumpling only: the inversion of δV between Fe-fcc and Fe-hcp sites in nonpseudomorphic and pseudomorphic models is not driven by the corresponding inversion of the FeO rumpling. We note that the average potential at large distance from the surface $\langle V \rangle_\infty$ is also sensitive to the choice of interface model: $\langle V \rangle_\infty = -0.4$ and $+0.1$ eV, respectively, for the NP1 and NP2 cells. This difference is consistent with a smaller average adsorption height (smaller interface dipole moment) in the NP2 model.

To summarize, our computational results reproduce satisfactorily the observed contrast in the STM images taken in the field emission mode and enable an identification of the physical origin of the observed modulation of the work function in the Moiré cell. We find that its site dependence is driven mainly by the local geometry of the FeO layer: rumpling and adsorption height. While the particular geometry of the Fe-top site results in a well-pronounced minimum of the work function, the differences between Fe-fcc and Fe-hcp sites are much less pronounced and rather model dependent. Indeed, by comparing the results from various pseudomorphic and NP models, we show that small differences of local and average adsorption heights may considerably affect the calculated work functions.

3. STM images

STM topographic images of the FeO layer, Fig. 5, reveal the hexagonal Moiré pattern originating from the 11% lattice mismatch with the Pt(111) support (marked by a dashed line in Fig. 5). Within the Moiré unit cell, different domains can be distinguished on the basis of their characteristic contrast evolution as a function of sample bias. At 65 mV, the domains marked by a square (attributed to fcc stacking) appear the brightest, while at 500 mV, the triangular regions (assigned to hcp stacking) dominate the sample topography. Circular regions corresponding to Fe-top sites are imaged as deep holes in the low bias range. With further bias increase, the circular regions gradually gain height and appear brightest in images taken above 750 mV. This radical contrast reversal is accompanied by a sharp increase in the differential conductance at 500 mV for this FeO domain, as obtained by spectroscopic measurements (not shown).

In the past, Galloway *et al.*[32] have already simulated STM images of the FeO/Pt(111) at 30 mV bias with an electron-scattering approach. They identified the leading electronic contribution given by the mixing of Fe d_{z2} and O p_z orbitals, which overrides the purely geometrical effects due to the differences of adsorption heights. This contribution was found to be responsible for the enhanced brightness of the Fe-hcp region, in contrast to the experimental findings where the fcc-region appears brightest in low bias images.

In order to explain the origin of the successive contrast evolution as a function of bias for the three regions in the Moiré cell, we have simulated STM images with the Tersoff-Hamann approach[57] at bias ranging from 65 to 1500 mV, Fig. 6. For the reasons discussed below, only the NP2 model has been used. In Fig. 7 we also present the decomposed LDOS, calculated in the vicinity of the Fermi level for the Fe d_{z2} and O p_z orbitals of atoms in the three regions of the supercell.

In agreement with the experimental findings, Figs. 5(b) and 5(c), our simulated images show a well pronounced contrast reversal between the Fe-hcp region which is the brightest below 600 mV and the Fe-top region which is imaged as a hole at low bias and becomes by far the brightest at high bias. As it can be seen in Fig. 7, this effect is principally driven by the Fe d_{z2} contribution, characterized by a large LDOS peak at about 0.7 eV above the Fermi level. The particularity of the Fe-top region originates from an enhanced overlap between Pt and Fe d_{z2} orbitals, responsible for the position of this LDOS structure. We note that this electronic

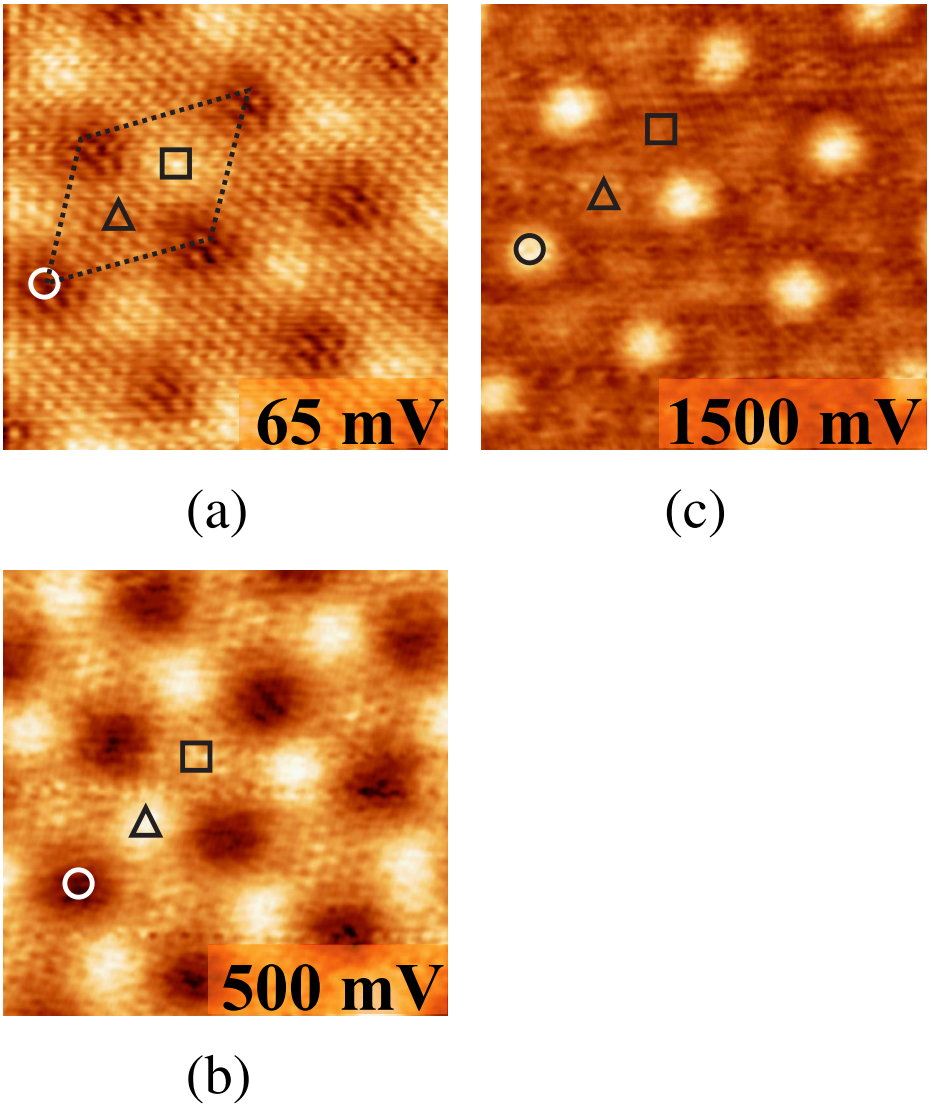

FIG. 5. (Color online) STM topographic images of FeO on Pt(111) taken at the bias voltages indicated in the images (I_t=0.1 nA, 8.6×8.6 nm^2). The symbols mark the different stacking domains within the FeO Moiré cell (Fe-top, circle; Fe-hcp, triangle; Fe-fcc, square). (a) Bias V=65 mV; (b) Bias V=500 mV; (c) Bias V=1500 mV.

effect is additionally enhanced by a geometrical one—the interface separation is by far the largest in the Fe-top configuration. At this point it is worth noting that the very same transition occurs already at less than 100 mV in STM images obtained from the NP1 model (not shown). This is a consequence of a lower energy of the dominant LDOS peak in the Fe d_{z2} contribution, driven by a larger interface separation (due to the artificial lateral constraint on the Pt substrate).

For low bias images, the brightness of the different regions is determined mainly by the contribution of O p_z orbitals. In agreement with the study by Galloway *et al.*,[32] we find that the Fe-hcp site is characterized by larger LDOS in the vicinity of the Fermi level, due to an enhanced overlap between Pt and O orbitals (O-top site), which contributes strongly to the brightness of the Fe-hcp region in the calculated STM image. However, our results show that the detailed structure of LDOS is very sensitive to the local magnetic order in the FeO film. In particular, a local parallel spin alignment on the Fe ions results in a pronounced enhancement of O p_z LDOS close to the Fermi level, which may override the dominance of the Fe-hcp site and produce a Fe-fcc/Fe-hcp brightness reversal in the STM images calculated at a very low bias (not shown). While the detailed determination of the actual magnetic order in the experimental Moiré cell goes beyond the scope of the present study, we conclude that at lowest bias the magnetic effects may be responsible for the specific contrast observed in the experimental STM images, Figs. 5(a) and 5(b).

IV. CONCLUSIONS

We have studied the electronic and structural properties of a FeO/Pt(111) monolayer, which has also been the subject of a series of experimental studies.[13,26–32] Going beyond the existing theoretical results,[32–34] we have considered fully relaxed FeO structures, using both pseudomorphic and nonpseudomorphic models, and have explicitly taken into account the effects of the magnetic order in the oxide film.

We find a clear preference for an antiparallel alignment of the magnetic moments, which however does only moderately affect the structural characteristics of the supported oxide film. This is consistent with the experimental observation that the film is nonferromagnetic. We find a pronounced rumpling with an outward relaxation of the oxygen ions, coupled

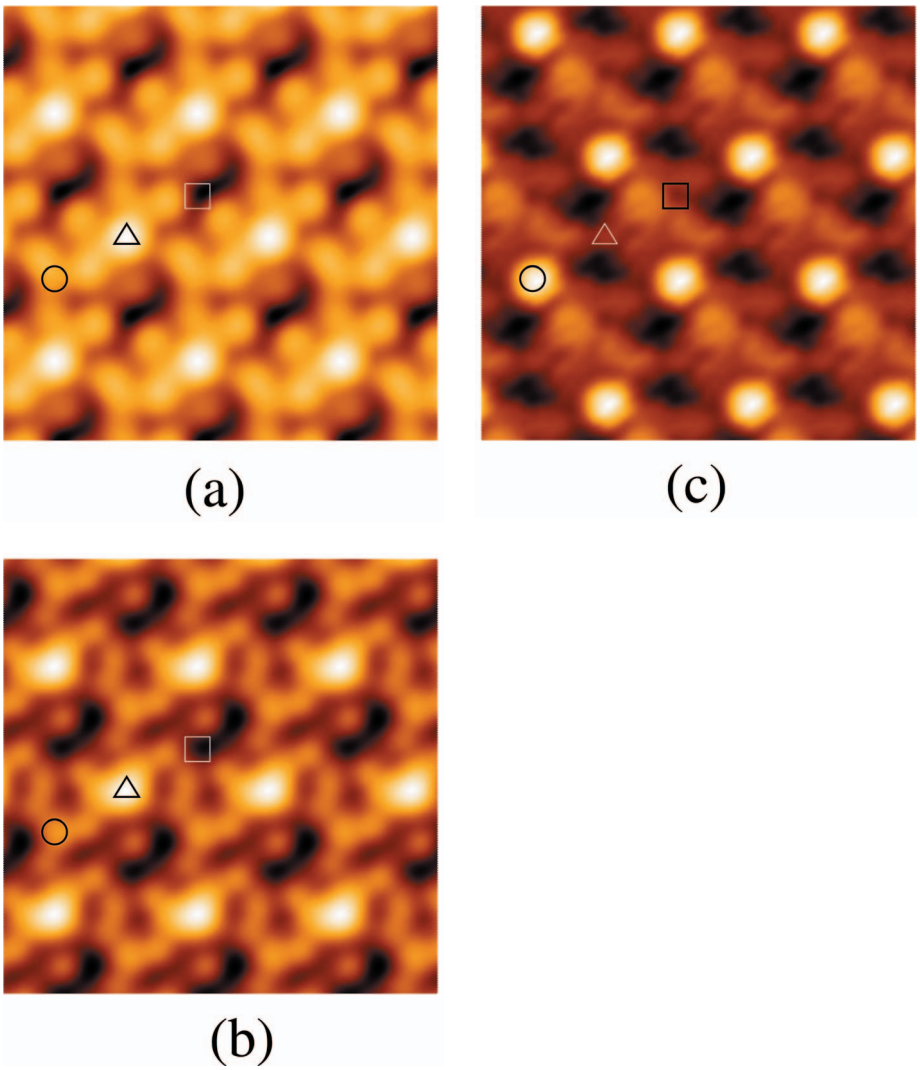

FIG. 6. (Color online) Simulated STM images of the antiferrimagnetic FeO/Pt(111) monolayer in the NP2 unit cell (2.5×2.5 nm^2). The symbols represent the position of the high-symmetry Fe ions: Fe-top (circle), Fe-hcp (triangle), and Fe-fcc (square), electron isodensity at 1×10^{-5} $e/$Å^3. (a) Bias $V=65$ mV. (b) Bias $V=500$ mV. (c) Bias $V=1500$ mV.

with an electron transfer towards the Pt substrate, which is practically independent of the local interface geometry and the magnetic order in the FeO film. Considering that the unsupported FeO(111) monolayer is flat, this relatively strong rumpling is entirely substrate induced. The modulation of the film structure is driven by the strength of the local interaction with the substrate. While adsorption in hollow sites results in a stronger FeO-Pt interaction, smaller interface separation, and larger rumpling, on the Fe-top sites the interaction is weak, the interface separation large, and the structural characteristics of the FeO film close to those of an unsupported film.

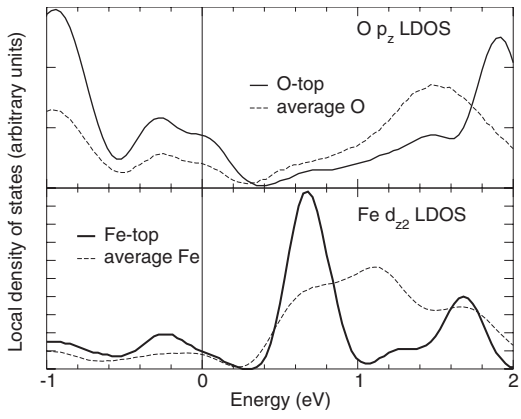

FIG. 7. Projected LDOS, calculated in the vicinity of the Fermi level. Top panel, O p_z orbitals; bottom panel, Fe d_{z2}. Solid lines, LDOS at specific sites of the Moiré pattern [O-top (Fe-fcc) and Fe-top of Pt atoms]; dashed lines, average LDOS.

The local interface geometry determines the main experimental observables of the FeO/Pt(111) layer. This is well exemplified by the peculiarity of the Fe-top site, where a large interface separation and a small layer rumpling determine a reduction of the work function, coherent with the most recent experimental findings. We also show that the main characteristics of the Fe d_{z2} and O p_z LDOS can be directly associated to the bias-dependent changes of the apparent height within the Moiré cell in experimental and calculated STM images. The main change between Fe-hcp and Fe-top sites is driven by a large Fe d_{z2} feature in the LDOS of the Fe-top region. The special position of this state with respect to the rest of the conduction band is due to a strong overlap of film and substrate orbitals. At low bias, the strong tunneling from the O-top region of Fe-hcp sites may be over-

ridden by effects induced by the local magnetic order in the FeO film.

Finally, while the peculiarity of the Fe-top geometry is qualitatively well accounted for by all considered models, we point out that finer characteristics (e.g., differentiation between Fe-hcp and Fe-fcc sites) and most of quantitative results (e.g., modification of the work function) are sensitive to the model of the interface. In particular, the calculated interface separation, which determines the sign of the work function change, depends on the magnetic order in the FeO film (ferromagnetic versus antiferromagnetic), on the type of the interface model (pseudomorphic versus nonpseudomorphic), and on the constraint of the substrate imposed to assure matching of the lattice parameters. Only antiferromagnetic, nonpseudomorphic interface models, with an unconstrained Pt substrate give results consistent with the experimental evidences.

ACKNOWLEDGMENTS

The authors thank C. Noguera for stimulating discussions. This work is supported by the European STRP project GSOMEN and by the European COST action D41 "Inorganic oxide surfaces and interfaces."

*Corresponding author; livia.giordano@mater.unimib.it

[1] Y. Motoyama, H. Matsuzaki, and H. Murakami, IEEE Trans. Electron Devices **48**, 1568 (2001).
[2] L. F. Weber, in *Flat-Panel Displays and CRTs*, edited by L. E. Tannas (Van Nostrand Reinhold, New York, 1985), Chap. 10.
[3] Y. T. Matulevich, T. J. Vink, and P. A. Zeijlmans van Emmichoven, Phys. Rev. Lett. **89**, 167601 (2002).
[4] S. S. P. Parkin, C. Kaiser, A. Panchula, P. M. Rice, B. Hughes, M. Samant, and S.-H. Yang, Nat. Mater. **3**, 862 (2004).
[5] S. Schintke and W.-D. Schneider, J. Phys.: Condens. Matter **16**, R49 (2004).
[6] S. A. Chambers, Surf. Sci. Rep. **39**, 105 (2000).
[7] G. Kresse, M. Schmid, E. Napetschnig, M. Shishkin, L. Köhler, and P. Varga, Science **308**, 1440 (2005).
[8] S. Agnoli, M. Sambi, G. Granozzi, J. Schoiswohl, S. Surnev, F. P. Netzer, M. Ferrero, A. M. Ferrari, and C. Pisani, J. Phys. Chem. B **109**, 17197 (2005).
[9] S. Altieri, L. H. Tjeng, and G. A. Sawatzky, Phys. Rev. B **61**, 16948 (2000).
[10] G. Pacchioni, L. Giordano, and M. Baistrocchi, Phys. Rev. Lett. **94**, 226104 (2005).
[11] M. Sterrer, T. Risse, U. Martinez Pozzoni, L. Giordano, M. Heyde, H. P. Rust, G. Pacchioni, and H.-J. Freund, Phys. Rev. Lett. **98**, 096107 (2007).
[12] H. Grönbeck, J. Phys. Chem. B **110**, 11977 (2006).
[13] G. H. Vurens, M. Salmeron, and G. A. Somorjai, Surf. Sci. **201**, 129 (1988).
[14] V. E. Henrich and P. A. Cox, *The Surface Science of Metal Oxides* (Cambridge University Press, Cambridge, UK, 1994).
[15] C. Noguera, *Physics and Chemistry at Oxide Surfaces* (Cambridge University Press, Cambridge, UK, 1996).
[16] A. Barbier, C. Mocuta, and G. Renaud, Phys. Rev. B **62**, 16056 (2000).
[17] B. Dillmann, F. Rohr, O. Seiferth, G. Klivenyi, M. Bender, K. Homann, I. N. Yakovkin, D. Ehrlich, M. Bäumer, H. Kuhlebeck, and H.-J. Freund, Faraday Discuss. **105**, 295 (1996).
[18] C. Noguera, J. Phys.: Condens. Matter **12**, R367 (2000), and references therein.
[19] F. Finocchi, A. Barbier, J. Jupille, and C. Noguera, Phys. Rev. Lett. **92**, 136101 (2004).
[20] J. Goniakowski and C. Noguera, Phys. Rev. B **60**, 16120 (1999).
[21] J. Goniakowski and C. Noguera, Phys. Rev. B **66**, 085417 (2002).
[22] M. Kiguchi, S. Entani, K. Saiki, T. Goto, and A. Koma, Phys. Rev. B **68**, 115402 (2003).
[23] R. Arita, Y. Tanida, S. Entani, M. Kiguchi, K. Saiki, and H. Aoki, Phys. Rev. B **69**, 235423 (2004).
[24] J. Goniakowski, C. Noguera, and L. Giordano, Phys. Rev. Lett. **93**, 215702 (2004).
[25] J. Goniakowski, C. Noguera, and L. Giordano, Phys. Rev. Lett. **98**, 205701 (2007).
[26] H. C. Galloway, J. J. Benítez, and M. Salmeron, Surf. Sci. **298**, 127 (1993).
[27] Y. J. Kim, C. Westphal, R. X. Ynzunza, H. C. Galloway, M. B. Salmeron, M. A. Van Hove, and C. S. Fadley, Phys. Rev. B **55**, R13448 (1997).
[28] Y. J. Kim, C. Westphal, R. X. Ynzunza, Z. Wang, H. C. Galloway, M. Salmeron, M. A. Van Hove, and C. S. Fadley, Surf. Sci. **416**, 68 (1998).
[29] M. Ritter, W. Ranke, and W. Weiss, Phys. Rev. B **57**, 7240 (1998).
[30] W. Ranke, M. Ritter, and W. Weiss, Phys. Rev. B **60**, 1527 (1999).
[31] E. D. L. Rienks, N. Nilius, H.-P. Rust, and H.-J. Freund, Phys. Rev. B **71**, 241404(R) (2005).
[32] H. C. Galloway, P. Sautet, and M. Salmeron, Phys. Rev. B **54**, R11145 (1996).
[33] Sh. K. Shaikhutdinov, R. Meyer, D. Lahav, M. Bäumer, T. Klüner, and H.-J. Freund, Phys. Rev. Lett. **91**, 076102 (2003).
[34] R. Meyer, D. Lahav, T. Schalow, M. Laurin, B. Brandt, S. Schauermann, S. Guimond, T. Klüner, H. Kuhlenbeck, J. Libuda, Sh. K. Shaikhutdinov, and H.-J. Freund, Surf. Sci. **586**, 174 (2005).
[35] N. Nilius, E. D. L. Rienks, H.-P. Rust, and H.-J. Freund, Phys. Rev. Lett. **95**, 066101 (2005).
[36] B. T. M. Willis and H. P. Rooksby, Acta Crystallogr. **6**, 827 (1953).
[37] S. Heinze, M. Bode, A. Kubetzka, O. Pietzsch, X. Nie, S. Blügel, and R. Wiesendanger, Science **288**, 1805 (2000).
[38] A. Kubetzka, P. Ferriani, M. Bode, S. Heinze, G. Bihlmayer, K. von Bergmann, O. Pietzsch, S. Blügel, and R. Wiesendanger, Phys. Rev. Lett. **94**, 087204 (2005).
[39] K. von Bergmann, S. Heinze, M. Bode, E. Y. Vedmedenko, G. Bihlmayer, S. Blügel, and R. Wiesendanger, Phys. Rev. Lett. **96**, 167203 (2006).
[40] I. I. Mazin and V. I. Anisimov, Phys. Rev. B **55**, 12822 (1997).

[41] Z. Fang, I. V. Solovyev, H. Sawada, and K. Terakura, Phys. Rev. B **59**, 762 (1999).
[42] S. A. Gramsch, R. E. Cohen, and S. Y. Savrasov, Am. Mineral. **88**, 257 (2003).
[43] M. Alfredsson, G. D. Price, C. R. A. Catlow, S. C. Parker, R. Orlando, and J. P. Brodholt, Phys. Rev. B **70**, 165111 (2004).
[44] M. Cococcioni and S. de Gironcoli, Phys. Rev. B **71**, 035105 (2005).
[45] Y. L. Li, K. L. Yao, Z. L. Liu, and G. Y. Gao, Phys. Rev. B **72**, 155446 (2005).
[46] S. L. Dudarev, G. A. Botton, S. Y. Savrasov, C. J. Humphreys, and A. P. Sutton, Phys. Rev. B **57**, 1505 (1998).
[47] G. Kresse and J. Hafner, Phys. Rev. B **47**, R558 (1993).
[48] G. Kresse and J. Furthmüller, Phys. Rev. B **54**, 11169 (1996).
[49] J. P. Perdew, J. A. Chevary, S. H. Vosko, K. A. Jackson, M. R. Pederson, D. J. Singh, and C. Fiolhais, Phys. Rev. B **46**, 6671 (1992).
[50] P. E. Blöchl, Phys. Rev. B **50**, 17953 (1994).
[51] O. Bengone, M. Alouani, P. E. Blöchl, and J. Hugel, Phys. Rev. B **62**, 16392 (2000).
[52] G. Rollmann, A. Rohrbach, P. Entel, and J. Hafner, Phys. Rev. B **69**, 165107 (2004).
[53] R. F. W. Bader, Chem. Rev. (Washington, D.C.) **91**, 983 (1991), as implemented in the ABINIT code by K. Casek, F. Finocchi, and X. Gonze.
[54] Ph. Kurz, G. Bihlmayer, K. Hirai, and S. Blügel, Phys. Rev. Lett. **86**, 1106 (2001).
[55] W. Vervisch, C. Mottet, and J. Goniakowski, Phys. Rev. B **65**, 245411 (2002).
[56] E. D. L. Rienks, N. Nilius, L. Giordano, J. Goniakowski, G. Pacchioni, M. P. Felicissimo, T. Risse, H.-P. Rust, and H.-J. Freund, Phys. Rev. B **75**, 205443 (2007).
[57] J. Tersoff and D. R. Hamann, Phys. Rev. B **31**, 805 (1985).
[58] M. Pivetta, F. Patthey, M. Stengel, A. Baldereschi, and W. D. Schneider, Phys. Rev. B **72**, 115404 (2005).
[59] L. Giordano, F. Cinquini, and G. Pacchioni, Phys. Rev. B **73**, 045414 (2006).
[60] J. Goniakowski and C. Noguera, Interface Sci. **12**, 93 (2004).